Observer-Based Asynchronous Control of Nonlinear Systems With Dynamic Event-Based Try-Once-Discard Protocol

Jun Cheng, Ju H. Park, *Senior Member, IEEE*, and Zheng-Guang Wu, *Member, IEEE*

***Abstract*—This work investigates the observer-based asynchronous control of discrete-time nonlinear systems with network-induced communication constraints. To avoid the data collisions and side effects in a constrained communication channel, a novel dynamic event-based weighted try-once-discard (DEWTOD) protocol is proposed. In contrast to the existing protocols, the DEWTOD scheduling regulates whether the sampling instant to release and which node to transmit the sampling instant simultaneously. In light of a hidden Markov model, the time-varying detection probability matrix is characterized by a polytopic set. By resorting to the polytopic-structured Lyapunov functional, sufficient conditions are derived such that the closed-loop dynamic is mean-square exponentially stable, and the observer-based controller is designed. In the end, two numerical examples are provided to explicate the validity of the attained methodology.**

***Index Terms*—Discrete-time, event-triggered, hidden Markov model, nonlinear system, try-once-discard protocol.**

I. Introduction

THE MARKOV switching systems (MSSs) have gained a steadily increasing interest in various physical applications, for instance, economic systems, multiagent systems, etc. In MSSs, the sudden changes are regulated by a Markov process. Therefore, MSSs consist of multiple operating models. Over the past few decades, extensive attention has been shifted to MSSs, and numerous theoretical results have been exhibited [1]–[7]. Note that when the system states are not accessible in many cases, the observer-based control law can be adapted to deal with the above shortage [8], [9]. Within this context, the filter/observer/controller is prescribed to be fully synchronous with the corresponding systems. Clearly, the aforementioned assumption is unrealistic due to many unknown factors (actuator/sensor failures) [10], [11], which limits the potential physical application. Therefore, it is natural to devote the research efforts to the nonsynchronous filter/observer/controller for MSSs. Recently, as discussed in [12], the asynchronous filters have been studied by using the partly actual mode information. Differently, the hidden Markov model strategy is a most welcome technique, where the operation mode can be evaluated via a detector [13]–[15]. By means of the hidden Markov model, tremendous results have been addressed in [16] and [17], which gives rise to the hidden Markov model design law. On the other hand, in the above circumstances, all the detection probabilities are assumed to be time invariant. In reality, by virtue of the detector, the detection probabilities can be varied arbitrarily or periodically. In light of these observations, constructing a comprehensive hidden Markov model in solving time-varying detection probabilities partially motivates the current study.

On the other hand, due to the advantages of lower cost, easier implementation, there has been a growing interest in networked control systems. In the networked control systems, due to its unreliability in data transmission, for saving the computation resource and improving the communication capacity, the event-triggered scheme (ETS) cannot be omitted. Compared to the conventional time-triggered scheme, the ETS releases certain information only when an event is activated [18]. Following this trend, the static ETS (SETS) has been studied [19]–[21]. With the aid of asynchronization phenomena, the static event-triggered asynchronous control/filtering for MSSs have been addressed [22], [23]. Very recently, by employing an extra internal dynamic parameter, the dynamic ETS (DETS) has been forwarded in [24] and [25]. Compared to the SETS, the dynamic case adjusts the event-triggering condition adaptively. As for asynchronous control/filtering of MSSs, the DETS has not gained suitable attention.

Besides, it is well acknowledged that constraint communication may lead to unpredictable phenomena including data collisions, which affect the networked system performance.

Manuscript received 20 January 2021; revised 17 May 2021; accepted 11 August 2021. Date of publication 30 August 2021; date of current version 18 November 2022. This work was supported in part by the National Natural Science Foundation of China under Grant 12161011 and Grant 62173100; in part by the National Natural Science Foundation of Guangxi Province under Grant 2020GXNSFAA159049 and Grant 2020GXNSFFA297003; in part by the Guangxi Science and Technology Base and Specialized Talents under Grant Guike AD20159057; and in part by the Training Program for 1000 Young and Middle-aged Cadre Teachers in Universities of Guangxi Province. The work of Ju H. Park was supported by the National Research Foundation of Korea (NRF) grant funded by the Korea Government (Ministry of Science and ICT) under Grant 2019R1A5A8080290. This article was recommended by Associate Editor C.-M. Lin. *(Corresponding authors: Jun Cheng; Ju H. Park.)*

Jun Cheng is with the School of Mathematics and Statistics, Center for Applied Mathematics of Guangxi, Guangxi Normal University, Guilin 541006, China, also with the School of Information Science and Engineering, Chengdu University, Chengdu 610106, China, and also with the Department of Electrical Engineering, Yeungnam University, Gyeongsan 38541, Republic of Korea (e-mail: jcheng@gxnu.edu.cn; jcheng6819@126.com).

Ju H. Park is with the Department of Electrical Engineering, Yeungnam University, Gyeongsan 38541, Republic of Korea (e-mail: jessie@ynu.ac.kr).

Zheng-Guang Wu is with the Institute of Cyber-Systems and Control, Zhejiang University, Hangzhou 310027, China (e-mail: nashwzhg@zju.edu.cn).

Color versions of one or more figures in this article are available at https://doi.org/10.1109/TCYB.2021.3104806.

Digital Object Identifier 10.1109/TCYB.2021.3104806

Thankfully, the communication protocols have been adopted to regulate the order of data transmissions, such as the event-triggering protocol [26]; round-robin protocol [27]; random access protocol [28]; and weighted try-once-discard (WTOD) protocol [29], [30]. Note that the round-robin protocol is the simplest, which has been known as a static transmission volume. Compared to the former protocols, the WTOD protocol is a superior case, which schedules behaviors in a dynamic way. Nevertheless, due to the changes in the data communication order, the WTOD protocol may result in side effects, which requires further investigation. Meanwhile, although the WTOD protocol is quite effective in scheduling the actuator/sensor node via a maximum-error-fist order, it cannot be applied to alleviate the transmission burden since the dispensable data are transmitted through a constraint communication network. In light of the capacity of communication channels, it is naturally curious whether we can propose a novel communication protocol in alleviating the data transmission burden and avoiding data congestions, simultaneously? The lack of guidance in tackling the aforementioned issue motivates us to shorten such a gap.

Motivated by the above discussion, it is imperative to investigate the asynchronous filtering of MSS with dynamic event-based WTOD (DEWTOD) protocol. The main contribution can be summarized as below.

1) Considering the asynchronous phenomena, the hidden Markov model with time-varying detection probabilities is absorbed, and the time-varying detection probability matrix is characterized by a polytopic set.
2) To avoid the side effects of the filter design, a novel DEWTOD protocol is forwarded to determine whether the sampling instant is to release and which node to transmit the sampling instant simultaneously.
3) Added by the hidden Markov model, the asynchronous observer-based controller gains are obtained in the sense of mean-square exponentially stable (MSES).

In summary, for the purpose of mitigating the communication burden and arranging the transmission order efficiently, a novel DEWTOD protocol is proposed for the networked MSSs. A key feature of the DEWTOD protocol is that it can be adopted to decide whether the sampling instant to release and which node to transmit the sampling instant simultaneously. Essentially different from most existing literature, by virtue of the hidden Markov model and the polytope-structured model, the asynchronous observer-based controller with time-varying detection probabilities is developed. Based on the Lyapunov theory, sufficient conditions that guarantee the resulting dynamic is stochastically stable are derived. In the end, two numerical examples are presented to explicate the validity of the gained results.

The remainder of this study is organized as follows. The model description with the DEWTOD protocol and asynchronous observer-based controller is displayed in Section II. The main results are expressed in Section III. Two practical examples are presented in Section IV. Eventually, the conclusion is summarized in Section V.

Notations: The notations of this study are standard. $\mathbb{R}^{a\times b}$ indicates $a \times b$-dimensional Euclidean space. $I_{a\times a}$ means a-dimensional identity. $\mathrm{tr}\{\mathscr{Q}\}$ indicates the trace of $\mathscr{Q}$. $\|\delta\|_{\mathscr{Q}}$ stands for the weighted norm of δ : $\|\delta\|_{\mathscr{Q}} = \sqrt{\delta^\top \mathscr{Q} \delta}$. $\mathrm{sym}\{\mathscr{Q}\} = \mathscr{Q} + \mathscr{Q}^\top$, $\mathscr{E}\{\cdot\}$ is the conditional expectation operator. $\lambda_{\min}(\mathscr{Q})$ and $\lambda_{\max}(\mathscr{Q})$, respectively, represent the minimum and maximum eigenvalue of $\mathscr{Q}$. $\arg\max_{x_1 \le x \le x_2}(f(x))$ being a function that spot the independent scalar $x \in [x_1, x_2]$ corresponded to the maximum value of $f(x)$. $*$ represents the symmetrical part of matrix.

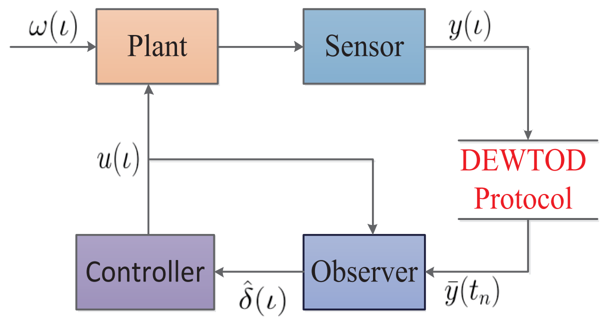

Fig. 1. Structure of the observer-based MSS.

II. Problem Formulation

A. Model Description

Consider the following discrete-time MSSs:

$$\begin{cases} \delta(\iota+1) = A(\alpha_\iota)\delta(\iota) + B(\alpha_\iota)u(\iota) + E(\alpha_\iota)\omega(\iota) \\ y(\iota) = C(\alpha_\iota)\delta(\iota) \\ z(\iota) = F(\alpha_\iota)\delta(\iota) \end{cases} \tag{1}$$

where $\delta(\iota) \in \mathbb{R}^{n_\delta}$ express the state vector, $y(\iota) \in \mathbb{R}^{n_y}$ signifies the measurement signal, and $z(\iota) \in \mathbb{R}^{n_z}$ symbolizes the control output signal. $\omega(\iota) \in \mathbb{R}^{w}$ indicates the disturbance input. The matrices $A(\alpha_\iota)$, $B(\alpha_\iota)$, $C(\alpha_\iota)$, $E(\alpha_\iota)$, and $F(\alpha_\iota)$ are known matrices with suitable dimensions.

In MSS (1), the switching parameter $\alpha_\iota \in \mathcal{S}_s = \{1, 2, \ldots, S_s\}$ is assumed to be a discrete-time Markov process (DTMP), which regulates values over a set $\mathcal{S}_s$. Meanwhile, the transition probability matrix of DTMP α_ι is given by $\Pi = [\varphi_{pq}]_{\mathcal{S}_s\times\mathcal{S}_s}$

$$\varphi_{pq} = \Pr\{\alpha_{\iota+1} = q | \alpha_\iota = p\} \tag{2}$$

where $\forall p, q \in \mathcal{S}_s$, $\varphi_{pq} \in [0, 1]$, and $\sum_{q\in\mathcal{S}_s} \varphi_{pq} = 1$.

B. DEWTOD Protocol

In networked control systems, the sensor and controller are connected through a shared communication network. For the purpose of saving limited computer resources, a special DEWTOD protocol is illustrated. As sketched in Fig. 1, the DEWTOD protocol is more general than the existing ones by scheduling the data communication in a dynamic way. More specifically, selecting an event-released time sequence $\{t_n, n = 1, 2, \ldots,\}$, and defining an dynamic generator function $f(\cdot)$ in the form of

$$f(\iota, \eta, \upsilon) = \frac{1}{\eta}\Im(\iota) + \upsilon y^\top(\iota)y(\iota) - \varepsilon^\top(\iota)\varepsilon(\iota) \tag{3}$$

where $\varepsilon(\iota) = y(\iota) - y(t_n)$. $y(t_n)$ denotes the latest triggered measurement output and $y(\iota)$ symbolizes the current measurement. $\eta > 0$ and $\upsilon > 0$ are given scalars. $\Im(\iota)$ in (3) is an internal dynamic state and satisfies

$$\begin{cases} \Im(\iota+1) = \theta\Im(\iota) + \upsilon y^\top(\iota)y(\iota) - \varepsilon^\top(\iota)\varepsilon(\iota) \\ \Im(0) = \Im \end{cases} \tag{4}$$

where the initial value $\Im \geq 0$ and $\theta \in (0, 1)$ being a given scalar. Benefitting from internal dynamic state $\Im(\iota)$, the threshold triggering parameter in (3) can be dynamically adjusted, which captures a wider physical applications than the ETS.

Generally, we rewrite the latest triggered measurement output $y(t_n) = [y_1^\top(t_n)\ y_2^\top(t_n)\ \cdots\ y_{n_y}^\top(t_n)]^\top$, where $y_i(t_n)$ symbolizes the latest triggered measurement output of the ith sensor. The received measurement is represented by $\bar{y}(t_n) = [\bar{y}_1^\top(t_n)\ \bar{y}_2^\top(t_n)\ \cdots\ \bar{y}_{n_y}^\top(t_n)]^\top$. By the DEWTOD protocol strategy, only one sensor is activated to access the communication network if and only if the following condition satisfied:

$$\bar{y}_i(\iota) = \begin{cases} \bar{y}_i(t_n), \text{ if } t_n = \min\{k \mid k > t_{n-1}, f(\iota,\eta,\upsilon) \leq 0\} \\ 0, \qquad \text{otherwise} \end{cases} \tag{5}$$

where

$$\bar{y}_i(t_n) = \begin{cases} y_i(t_n), & i = \zeta(t_n) \\ \bar{y}_i(t_{n-1}), & \text{otherwise.} \end{cases} \tag{6}$$

Specifically, the symbol $\zeta(t_n)$ means the activated sensor node at time-triggering interval t_n. In (4), $\zeta(t_n)$ takes the value in the set $\{1, 2, \ldots, n_y\}$, which is governed by the following principle:

$$\begin{aligned} \zeta(t_n) = \arg\max_{1\leq i\leq n_y} &\big(y_i(t_n) - \bar{y}_i(t_{n-1})\big)Q_i \\ &\times \big(y_i(t_n) - \bar{y}_i(t_{n-1})\big) \end{aligned} \tag{7}$$

where $\bar{y}_i(t_{n-1})$ is the previously transmitted data of node i at time instant t_n. $Q_i > 0 (1 \leq i \leq n_y)$ represents the weight matrix of the ith sensor node with $\sum_{i=1}^{n_y} Q_i = 1$. It can be observed from the WTOD protocol (5) that one sensor node is activated in the case of multiple nodes have the same maximal values.

To model the transmission mechanism of nodes mathematically, a Kronecker sign function is utilized

$$\phi(i) = \begin{cases} 1, & i = 0 \\ 0, & i \neq 0. \end{cases}$$

For $\forall 1 \leq i \leq n_y$, denoting $\Phi_i \triangleq \mathrm{diag}\{\phi(i-1), \phi(i-2), \ldots, \phi(i-n_y)\}$, the overall WTOD protocol is reformulated as

$$\begin{aligned} \zeta(t_n) = \arg\max_{1\leq i\leq n_y} &(y(t_n) - \bar{y}(t_{n-1}))\overline{Q}_i \\ &\times (y(t_n) - \bar{y}(t_{n-1})) \end{aligned} \tag{8}$$

where $\overline{Q}_i \triangleq \overline{Q}\Phi_i$, $\overline{Q} \triangleq \mathrm{diag}\{Q_1, Q_2, \ldots, Q_{n_y}\}$.

Inspired by the above observation, one concludes that when $t_n = \iota$, the ith sensor node $y_i(\iota)$ is released; otherwise, $t_n = t_{n-1} < k$. Therefore, the received measurement $\bar{y}(t_n)$ can be updated as

$$\bar{y}(t_n) = \begin{cases} 0, \qquad \iota < t_n \\ \Phi_{\zeta(t_n)}y(t_n) + \big(I_{n_y} - \Phi_{\zeta(t_n)}\big)\bar{y}(t_{n-1}) \\ \qquad \forall \iota \in \big[t_n, t_{n+1}\big),\ n \geq 0. \end{cases} \tag{9}$$

Remark 1: To relieve the constraint computation resources and avoid possible data collisions, a novel DEWTOD protocol is proposed in regulating the signal transmissions. By resorting to DEWTOD, a dynamic event trigger schedules the error and determines whether to release the measurement, and the WTOD protocol governs which measurement to be released. In spite of saving energy in the network channel, the conventional SETS and DETS may also lead to data collisions. Compared to the conventional SETM and DETM, the DEWTOD in this study is simultaneously improving the network utilization and reducing the transmission frequency.

Remark 2: Remarkably, in the DEWTOD protocol (3), the triggering condition $f(\iota, \eta, \upsilon) > 0$ is always holds, which signifies $\upsilon\|y(\iota)\|^2 - \|\varepsilon(\iota)\|^2 > -[1/\eta]\Im(\iota)$. Obviously, by the dynamical parameter $\Im(\iota)$, the triggering threshold can be dynamical adjusted. Clearly, one has $\Im(\iota+1) > (\theta - [1/\eta])\Im(\iota)$. For $\forall \iota > 0$, $\Im(\iota) > 0$ can be guaranteed if the inequalities $\theta\eta > 1$ and $\Im(0) > 0$ hold. Due to the internal dynamic state $\Im(\iota)$, the inequality $\upsilon\|y(\iota)\|^2 > \|\varepsilon(\iota)\|^2$ cannot be hold all the time. As implied in [25], letting $\eta \to \infty$, the consulting DEWTOD protocol will be degenerated to the SETS-based case. Furthermore, if $\eta \to \infty$ and $\theta = 0$, it reduces to the time-triggering scheme. Compared to the SETS and time-triggering scheme, the DEWTOD protocol may result in a larger value of the releasing interval.

C. Asynchronous Observer-Based Controller

In reality, the actual mode information may be unavailable to the observer. In response to the above phenomena, a mode detector is adopted to evaluate the actual mode information α_ι. Benefitting from the hidden Markov model, an observed mode $\beta_\iota \in \mathcal{S}_c = \{1, 2, \ldots, S_c\}$ is given, and the mode detection probability matrix $\Psi(\iota) = [\psi_{bg}(\iota)]_{S_c\times S_c}$ satisfies

$$\psi_{pg}(\iota) = \Pr\{\beta_\iota = g \mid \alpha_\iota = p\} \quad \forall g \in \mathcal{S}_c$$

where $\psi_{pg}(\iota)$ is the time-varying TP, and $\psi_{pg}(\iota) \geq 0$, $\sum_{g\in\mathcal{S}_f} \psi_{pg}(\iota) = 1$. Before further proceeding, we employ the function $\chi^l(\iota) (l \in \{1, 2, \ldots, L\})$

$$\chi^l(\iota) \geq 0, \quad \sum_{l=1}^{L} \chi^l(\iota) = 1. \tag{10}$$

Remarkably, the transition probability matrix $\Psi(\iota)$ can be expressed in a polytope structure set

$$\Psi(\iota) = \Psi(\chi(\iota)) = \sum_{l=1}^{L} \chi^l(\iota)\Psi^l \tag{11}$$

where $\chi(\iota) = [\chi^1(\iota)\ \chi^2(\iota)\ \cdots \chi^L(\iota)]$ and $\Psi^l = [\psi_{pg}^l]$ $(l \in \{1, 2, \ldots, L\}$. Similarly, the entry $\psi_{pg}(\iota)$ of $\Psi(\iota)$ obeys $\psi_{pg}(\iota) = \sum_{l=1}^{L} \chi^l(\iota)\psi_{pg}^l$.

Remark 3: Remarkably, by means of the hidden Markov model, the conditional probability in [13]–[15] is assumed to be time invariant. Differently, the conditional probability $\psi_{pg}(\iota)$ in this study is identified as nonhomogeneous, which relies on the current moment. Consequently, a polytope-structured model is addressed to depict the time-varying property, which covers the piecewise homogeneous conditional probability and homogeneous one as special cases.

In this study, the asynchronous observer-based controller is constructed as

$$\begin{aligned}\widehat{\delta}(\iota+1) &= A(\beta_\iota)\widehat{\delta}(\iota) + B(\beta_\iota)u(\iota)\\ &\quad + L(\beta_\iota,\zeta(t_n))\big(\bar{y}(t_n) - C(\beta_\iota)\widehat{\delta}(\iota)\big)\\ u(\iota) &= K(\beta_\iota,\zeta(t_n))\widehat{\delta}(\iota)\end{aligned} \tag{12}$$

where $\widehat{\delta}(\iota)$ portrays the state vector of the observer, and the matrices $L(\beta_\iota,\zeta(t_n))$ and $K(\beta_\iota,\zeta(t_n))$ are the observer and the controller parameters to be solved.

Defining the observer error $e(\iota) \triangleq \delta(\iota) - \widehat{\delta}(\iota)$, by MSS (8), the error system (13) is established

$$\begin{aligned}e(\iota+1) &= (A(\alpha_\iota) - L(\beta_\iota,\zeta(t_n))C(\alpha_\iota))e(\iota)\\ &\quad + L(\beta_\iota,\zeta(t_n))\big(I_{n_y} - \Phi_{\zeta(t_n)}\big)\\ &\quad \times (C(\alpha_\iota)\delta(\iota) - \bar{y}(t_{n-1})) + L(\beta_\iota,\zeta(t_n))\Phi_{\zeta(t_n)}\varepsilon(\iota)\\ &\quad + E(\iota)\omega(\iota).\end{aligned} \tag{13}$$

Denoting variable $\vartheta(\iota) = [\delta^\top(\iota) \quad \bar{y}^\top(t_{n-1}) \quad e^\top(\iota)]^\top$, the closed-loop MSS can be reformulated as

$$\begin{aligned}\vartheta(\iota+1) &= \mathcal{A}_{pg\zeta(t_n)}\vartheta(\iota) + \mathcal{B}_{pg\zeta(t_n)}\varepsilon(\iota) + \mathcal{C}_p\omega(\iota)\\ z(\iota) &= \mathcal{F}_p\vartheta(\iota)\end{aligned} \tag{14}$$

where

$$\mathcal{A}_{pg\zeta(t_n)} = \begin{bmatrix} A_p+B_pK_{g,\zeta(t_n)} & 0 & -B_pK_{g,\zeta(t_n)}\\ \Phi_{\zeta(t_n)}C_p & I_{n_y}-\Phi_{\zeta(t_n)} & 0\\ \mathcal{L}_{g,\zeta(t_n)}C_p & -\mathcal{L}_{g,\zeta(t_n)} & A_p-L_{g,\zeta(t_n)}C_p\end{bmatrix}$$

$$\mathcal{B}_{pg\zeta(t_n)} = \begin{bmatrix} 0\\ -\Phi_{\zeta(t_n)}\\ L_{g,\zeta(t_n)}\Phi_{\zeta(t_n)}\end{bmatrix}, \mathcal{F}_p = [F_p \quad 0 \quad 0]$$

$$\mathcal{C}_p = \begin{bmatrix} E_p\\ 0\\ E_p\end{bmatrix}, \mathcal{L}_{g,\zeta(t_n)} = L_{g,\zeta(t_n)}\big(I - \Phi_{\zeta(t_n)}\big).$$

Definition 1 [31]: The closed-loop dynamic (14) is called MSES, if there exist scalars $\nu_1 > 0$, $\nu_2 \in (0,1)$, such that

$$\mathscr{E}\Big\{\|\vartheta(\iota)\|^2 \le \nu_1\nu_2^\iota\mathscr{E}\Big\{\|\vartheta(0)\|^2\Big\},\ \iota \ge 0$$

holds for any initial condition $\vartheta(0)$.

Under the above conditions, the main purpose of this work is outlined as follows: for operation system (8), there exists a parameter γ, and $\omega(\iota) \in l_2[0,\infty)$, an asynchronous observer-based controller (12) is designed to guarantee the MSES of closed-loop dynamic (14), and $z(\iota)$ yields

$$\sqrt{\sum_{\iota=0}^{\infty}\|z(\iota)\|^2} \le \gamma\sqrt{\sum_{\iota=0}^{\infty}\|\omega(\iota)\|^2}.$$

Lemma 1 [32]: If there exist a parameter $\epsilon > 0$ and matrices $\{Z_s\}_{s=1}^4$ satisfied with the following condition:

$$\begin{bmatrix} Z_1 & Z_2 + Z_3^\top\\ * & \mathrm{sym}\{-\epsilon Z_4\}\end{bmatrix} < 0$$

then the following condition holds:

$$Z_1 + \mathrm{sym}\Big\{Z_2Z_4^{-1}Z_3\Big\} < 0.$$

III. Main Results

In this section, the MSES of the closed-loop dynamic (14) will be presented, and the observer-based controller gains will be attained.

Theorem 1: Consider the discrete-time MSS (14) with the DEWTOD protocol. The closed-loop MSS (14) is MSES if, for given scalars $\theta > 0$ and $\eta > 0$, if conditions (1) and (2) meet

$$\theta\eta \ge 1 \tag{15}$$

and for any $p, q \in \mathcal{S}_s$, $g \in \mathcal{S}_c$, $\zeta(t_n) \in \{1,2,\ldots,n_y\}$, and $f, l \in \{1,2,\ldots,L\}$, there exist matrices $P_p^{(f)} > 0$, $R_{pg} > 0$, and matrix $\mathcal{X}_{g\zeta(t_n)}$, such that

$$-P_p^{(l)} + \sum_{g\in\mathcal{S}_c}\psi_{pg}^{(l)}R_{pg} < 0, \tag{16}$$

$$\begin{bmatrix} \Upsilon_{pg\zeta(t_n)} & \Omega_{pg\zeta(t_n)}\\ * & \Sigma_{fg\zeta(t_n)}\end{bmatrix} < 0 \tag{17}$$

where

$$\Upsilon_{pg\zeta(t_n)} = \begin{bmatrix} \Upsilon_{pg\zeta(t_n)}^{11} & \Upsilon_{pg\zeta(t_n)}^{12} & 0 & 0\\ * & \Upsilon_{pg\zeta(t_n)}^{22} & 0 & 0\\ * & * & \Upsilon_{pg\zeta(t_n)}^{33} & 0\\ * & * & * & \Upsilon_{pg\zeta(t_n)}^{44}\end{bmatrix}$$

$$\Omega_{pg\zeta(t_n)} = \Big[\Omega_{pg\zeta(t_n)}^{1\top} \quad \Omega_{pg\zeta(t_n)}^{2\top} \quad \Omega_{pg\zeta(t_n)}^{3\top} \quad 0\Big]^\top$$

$$\begin{aligned}\Sigma_{fg\zeta(t_n)} &= \mathrm{diag}\Big\{P_1^{(f)} - \mathbf{sym}\{\mathcal{X}_{g\zeta(t_n)}\}, \ldots, P_{S_s}^{(f)}\\ &\quad - \mathbf{sym}\{\mathcal{X}_{g\zeta(t_n)}\}\Big\}\end{aligned}$$

$$\Omega_{pg\zeta(t_n)}^1 = \Big[\sqrt{\varphi_{p1}}\mathcal{A}_{pg\zeta(t_n)}^\top\mathcal{X}_{g\zeta(t_n)}^\top \quad \cdots \quad \sqrt{\varphi_{pS_s}}\mathcal{A}_{pg\zeta(t_n)}^\top\mathcal{X}_{g\zeta(t_n)}^\top\Big]$$

$$\Omega_{pg\zeta(t_n)}^2 = \Big[\sqrt{\varphi_{p1}}\mathcal{B}_{pg\zeta(t_n)}^\top\mathcal{X}_{g\zeta(t_n)}^\top \quad \cdots \quad \sqrt{\varphi_{pS_s}}\mathcal{B}_{pg\zeta(t_n)}^\top\mathcal{X}_{g\zeta(t_n)}^\top\Big]$$

$$\Omega_{pg\zeta(t_n)}^3 = \Big[\sqrt{\varphi_{p1}}\mathcal{C}_p^\top\mathcal{X}_{g\zeta(t_n)}^\top \quad \cdots \quad \sqrt{\varphi_{pS_s}}\mathcal{C}_p^\top\mathcal{X}_{g\zeta(t_n)}^\top\Big]$$

$$\begin{aligned}\Upsilon_{pg\zeta(t_n)}^{11} &= -R_{pg} + \mathscr{C}_p^{2\top}\sum_{t=1}^{n_y}\kappa_{\zeta(t_n)t}\overline{Q}\big(\Phi_{\zeta(t_n)} - \Phi_t\big)\mathscr{C}_p^2\\ &\quad + \left(\frac{\upsilon}{\eta} + \sigma\upsilon\right)\mathscr{C}_p^{1\top}\mathscr{C}_p^1 + \mathcal{F}_p^\top\mathcal{F}_p\end{aligned}$$

$$\Upsilon_{pg\zeta(t_n)}^{12} = -\mathscr{C}_p^{2\top}\sum_{t=1}^{n_y}\kappa_{\zeta(t_n)t}\overline{Q}\big(\Phi_{\zeta(t_n)} - \Phi_t\big)$$

$$\Upsilon_{pg\zeta(t_n)}^{22} = \sum_{t=1}^{n_y}\kappa_{\zeta(t_n)t}\overline{Q}\big(\Phi_{\zeta(t_n)} - \Phi_t\big) - \left(\frac{1}{\eta} + \sigma\right)I$$

$$\Upsilon_{pg\zeta(t_n)}^{33} = -\gamma^2 I, \Upsilon_{pg\zeta(t_n)}^{44} = \frac{\theta + \sigma - 1}{\eta}I$$

$$\mathscr{C}_p^1 = \big[C_p \quad 0 \quad 0\big], \mathscr{C}_p^2 = \big[C_p \quad -I \quad 0\big].$$

Proof: In light of inequality $(\mathcal{X}_{g\zeta(t_n)} - \mathcal{P}_p^{(f)})(\mathcal{P}_p^{(f)})^{-1}(\mathcal{X}_{g\zeta(t_n)}^\top - \mathcal{P}_p^{(f)}) \ge 0$ holds, one has $-\mathcal{P}_p^{(f)} + \mathbf{sym}\{\mathcal{X}_{g\zeta(t_n)}\} \le \mathcal{X}_{g\zeta(t_n)}(\mathcal{P}_p^{(f)})^{-1}\mathcal{X}_{g\zeta(t_n)}^{-\top}$. Consequently, (17) can be reestablished as

$$\begin{bmatrix} \Upsilon_{pg\zeta(t_n)} & \overline{\Omega}_{pg\zeta(t_n)}\\ * & -\mathcal{X}_{g\zeta(t_n)}\Big(\mathcal{P}_p^{(f)}\Big)^{-1}\mathcal{X}_{g\zeta(t_n)}^{-\top}\end{bmatrix} < 0 \tag{18}$$

where $\overline{\Omega}_{pg\zeta(t_n)} = [\mathcal{A}_{pg\zeta(t_n)} \quad \mathcal{B}_{pg\zeta(t_n)} \quad \mathcal{C}_p \quad 0]^\top$ and $\mathcal{P}_p^{(f)} = \sum_{q\in\mathcal{S}_s} \varphi_{pq} P_q^{(f)}$. ■

Premultiplying and postmultiplying (18) with $\text{diag}\{I, I, I, \mathcal{P}_p^{(f)} \mathcal{X}_{g\zeta(t_n)}^{-1}\}$ and its transpose, which yields

$$\begin{bmatrix} \Upsilon_{pg\zeta(t_n)} & \Omega_{pg\zeta(t_n)}^\top \mathcal{P}_p^{(f)} \\ * & -\mathcal{P}_p^{(f)} \end{bmatrix} < 0. \tag{19}$$

In what follows, construct a Lyapunov functional for dynamic (14) as below:

$$\mathcal{V}(\vartheta_\iota, \alpha_\iota) = \vartheta^\top(\iota)\mathscr{P}_{\alpha_\iota}(\chi(\iota))\vartheta(\iota) + \frac{1}{\eta}\Im(\iota) \tag{20}$$

where $\mathscr{P}_{\alpha_\iota}(\chi(\iota)) = \sum_{l=1}^{L} \chi^l(\iota) P_{\alpha_\iota}^{(l)}$.

In fact, due to the fact that $\sum_{l=1}^{L} \chi^l(\iota) = 1$, letting $\varpi^f(\iota) \triangleq \chi^l(\iota+1)$, one has

$$\sum_{l=1}^{L} \chi^l(\iota+1) P_{\alpha_{\iota+1}}^{(l)} = \sum_{s=1}^{L} \varpi^f(\iota) P_{\alpha_\iota}^{(f)}. \tag{21}$$

Let $\Delta\mathcal{V}(\iota) = \mathcal{V}(\vartheta_{\iota+1}, \alpha_{\iota+1}) - \mathcal{V}(\vartheta_\iota, \alpha_\iota)$. When $p = \alpha_\iota$, $q = \alpha_{\iota+1}$, and $g = \beta_\iota$, the difference of $\mathcal{V}(\vartheta_\iota, \alpha_\iota)$ can be calculated as

$$\begin{aligned}
\mathscr{E}\{\Delta\mathcal{V}(\iota)\} &= \mathscr{E}\Bigg\{\vartheta^\top(\iota+1) \sum_{q\in\mathcal{S}_s} \varphi_{pq} \mathscr{P}_q(\chi(\iota+1))\vartheta(\iota+1) \\
&\quad - \vartheta^\top(\iota) P_p \vartheta(\iota) + \frac{1}{\eta}\Im(\iota+1) - \frac{1}{\eta}\Im(\iota)\Bigg\} \\
&= \mathscr{E}\Bigg\{\sum_{g\in\mathcal{S}_c} \psi_{pg}(\iota)\big[\mathcal{A}_{pg\zeta(t_n)}\vartheta(\iota) + \mathcal{B}_{pg\zeta(t_n)}\varepsilon(\iota) \\
&\quad + \mathcal{C}_p\omega(\iota)\big]^\top \sum_{l=1}^{L} \chi^l(\iota+1)\mathcal{P}_p^{(l)} \\
&\quad \times \big[\mathcal{A}_{pg\zeta(t_n)}\vartheta(\iota) + \mathcal{B}_{pg\zeta(t_n)}\varepsilon(\iota) + \mathcal{C}_p\omega(\iota)\big] \\
&\quad - \vartheta^\top(\iota) P_p \vartheta(\iota) + \frac{\theta - 1}{\eta}\Im(\iota) \\
&\quad + \frac{\upsilon}{\eta}\vartheta^\top(\iota)\mathscr{C}_p^{1\top}\mathscr{C}_p^1\vartheta(\iota) - \frac{1}{\eta}\varepsilon^\top(\iota)\varepsilon(\iota)\Bigg\} \\
&= \mathscr{E}\Bigg\{\sum_{l=1}^{L} \chi^l(\iota) \sum_{g\in\mathcal{S}_c} \psi_{pg}^{(l)} \sum_{f=1}^{L} \varpi^f(\iota) \\
&\quad \times \big[\mathcal{A}_{pg\zeta(t_n)}\vartheta(\iota) + \mathcal{B}_{pg\zeta(t_n)}\varepsilon(\iota) + \mathcal{C}_p\omega(\iota)\big]^\top \\
&\quad \times \mathcal{P}_p^{(f)}\big[\mathcal{A}_{pg\zeta(t_n)}\vartheta(\iota) \\
&\qquad + \mathcal{B}_{pg\zeta(t_n)}\varepsilon(\iota) + \mathcal{C}_p\omega(\iota)\big] \\
&\quad - \vartheta^\top(\iota) P_p \vartheta(\iota) + \frac{\theta - 1}{\eta}\Im(\iota) \\
&\quad + \frac{\upsilon}{\eta}\vartheta^\top(\iota)\mathscr{C}_p^{1\top}\mathscr{C}_p^1\vartheta(\iota) - \frac{1}{\eta}\varepsilon^\top(\iota)\varepsilon(\iota)\Bigg\}.
\end{aligned} \tag{22}$$

Recalling (1) and (3), for any $\iota \in [t_n, t_{n+1})$, one has

$$\frac{1}{\eta}\Im(\iota) + \upsilon\vartheta^\top(\iota)\mathscr{C}_p^{1\top}\mathscr{C}_p^1\vartheta(\iota) - \varepsilon^\top(\iota)\varepsilon(\iota) \geq 0. \tag{23}$$

By virtue of the dynamical inequalities (2) and (15), the following condition holds:

$$\Im(\iota+1) \geq \left(\theta - \frac{1}{\eta}\right)\Im(\iota) \geq \cdots \geq \left(\theta - \frac{1}{\eta}\right)^{\iota+1} \Im(0). \tag{24}$$

Obviously, for $\forall\iota \geq 0$, when the initial state $\Im(0) \geq 0$, $\Im(\iota) \geq 0$ can be guaranteed by (24).

Recalling the DEWTOD principle (5), for $\forall t \in \{1, 2, \ldots, n_y\}$, one obtains

$$\Big(\mathscr{C}_p^2\vartheta(\iota) - \varepsilon(\iota)\Big)^\top \overline{Q}\big(\Phi_{\zeta(t_n)} - \Phi_t\big)\Big(\mathscr{C}_p^2\vartheta(\iota) - \varepsilon(\iota)\Big) \geq 0. \tag{25}$$

Clearly, (25) equivalents

$$\begin{aligned}
&\Big(\mathscr{C}_p^2\vartheta(\iota) - \varepsilon(\iota)\Big)^\top \sum_{t=1}^{n_y} \kappa_{\zeta(t_n)t} \overline{Q}\big(\Phi_{\zeta(t_n)} - \Phi_t\big) \\
&\quad \times \Big(\mathscr{C}_p^2\vartheta(\iota) - \varepsilon(\iota)\Big) \geq 0.
\end{aligned} \tag{26}$$

Synthesizing (22)–(26), one derives

$$\begin{aligned}
\mathscr{E}\{\Delta\mathcal{V}(\iota)\} &\leq \mathscr{E}\{\Delta\mathcal{V}(\iota)\} \\
&\quad + \sigma\left[\frac{1}{\eta}\Im(\iota) + \upsilon\vartheta^\top(\iota)\mathscr{C}_p^{1\top}\mathscr{C}_p^1\vartheta(\iota) - \varepsilon^\top(\iota)\varepsilon(\iota)\right] \\
&\quad + \Big(\mathscr{C}_p^2\vartheta(\iota) - \varepsilon(\iota)\Big)^\top \sum_{t=1}^{n_y} \kappa_{\zeta(t_n)t} \\
&\quad \times \overline{Q}\big(\Phi_{\zeta(t_n)} - \Phi_t\big)\Big(\mathscr{C}_p^2\vartheta(\iota) - \varepsilon(\iota)\Big).
\end{aligned} \tag{27}$$

When $\omega(\iota) = 0$, it can be elicited from (27) that there exists a scalar $\hbar > 0$, such that $\mathscr{E}\{\Delta\mathcal{V}(\iota)\} < -\hbar\|\vartheta(\iota)\|^2$. From $\iota = 0$ to ∞, we have $\mathscr{E}\{\|\vartheta(\iota)\|^2 \leq \nu_1\nu_2^\iota \mathscr{E}\{\|\vartheta(0)\|^2\}$, which signifies that the closed-loop dynamic (14) is MSES.

Introducing an index function $\mathscr{J}(\iota)$ as

$$\begin{aligned}
\mathscr{J}(\iota) &= \mathscr{E}\Big\{\Delta\mathcal{V}(\iota) + z^\top(\iota)z(\iota) - \gamma^2\omega^\top(\iota)\omega(\iota))\Big\} \\
&\leq \xi^\top(\iota) \sum_{l=1}^{L} \chi^l(\iota) \sum_{g\in\mathcal{S}_c} \psi_{pg}^{(l)} \sum_{f=1}^{L} \varpi^f(\iota)\Omega_{pg\zeta(t_n)}^\top \\
&\quad \times \mathcal{P}_p^{(f)}\Omega_{pg\zeta(t_n)}\xi(\iota) + \xi^\top(\iota)\overline{\Upsilon}_{lpg\zeta(t_n)}\xi(\iota)
\end{aligned} \tag{28}$$

where

$$\xi(\iota) = \Big[\vartheta^\top(\iota) \quad \varepsilon^\top(\iota) \quad \omega^\top(\iota) \quad \sqrt{\Im}^\top\Big]^\top$$

$$\overline{\Upsilon}_{lpg\zeta(t_n)} = \begin{bmatrix} \overline{\Upsilon}_{lpg\zeta(t_n)}^{11} & \Upsilon_{pg\zeta(t_n)}^{12} & 0 & 0 \\ * & \Upsilon_{pg\zeta(t_n)}^{22} & 0 & 0 \\ * & * & \Upsilon_{pg\zeta(t_n)}^{33} & 0 \\ * & * & * & \Upsilon_{pg\zeta(t_n)}^{44} \end{bmatrix}$$

$$\begin{aligned}
\overline{\Upsilon}_{lpg\zeta(t_n)}^{11} &= -P_p^{(l)} + \left(\frac{\upsilon}{\eta} + \sigma\upsilon\right)\mathscr{C}_p^{1\top}\mathscr{C}_p^1 + \mathcal{F}_p^\top\mathcal{F}_p \\
&\quad + \mathscr{C}_p^{2\top} \sum_{t=1}^{n_y} \kappa_{\zeta(t_n)t}\overline{Q}\big(\Phi_{\zeta(t_n)} - \Phi_t\big)\mathscr{C}_p^2.
\end{aligned}$$

With respect to the fact that $\sum_{l=1}^{L} \chi^l(\iota) = 1$, it follows from (16) that:

$$\sum_{l=1}^{L} \chi^l(\iota) \sum_{g\in\mathcal{S}_c} \psi_{pg}^{(l)} R_{pg} \leq P_p^{(l)}. \tag{29}$$

Under the polytopic principle, one derives

$$\mathscr{J}(\iota) \leq \xi^{\top}(\iota)\left\{\sum_{l=1}^{L}\chi^{l}(\iota)\sum_{s=1}^{L}\varpi^{s}(\iota)\sum_{g\in\mathcal{S}_c}\psi_{pg}^{l} \times\left[\Omega_{pg\zeta(t_n)}^{\top}\mathcal{P}_p^{(f)}\Omega_{pg\zeta(t_n)}+\Upsilon_{pg\zeta(t_n)}\right]\right\}\xi(\iota). \tag{30}$$

In light of the Schur complement, it can be elicited from (19) that $\mathscr{J}(\iota) < 0$. By Definition 1, one concludes the closed-loop MSS (14) is MSES with a predefined performance level γ. The proof is completed. ■

In the following section, by the proper matrix processing technique, the observer-based controller gains will be designed.

Theorem 2: Consider the discrete-time MSS (14) with the DEWTOD protocol. The closed-loop MSS (14) is MSES if, for given scalars $\theta > 0$ and $\eta > 0$, $\sigma > 0$, and $\epsilon > 0$, for any $p, q \in \mathcal{S}_s$, $g \in \mathcal{S}_c$, $\zeta(t_n) \in \{1, 2, \dots, n_y\}$, and $f, l \in \{1, 2, \dots, L\}$, there exist matrices $P_p^{(f)} = \begin{bmatrix} P_p^{1(f)} & P_p^{2(f)} & P_p^{3(f)} \\ * & P_p^{4(f)} & P_p^{5(f)} \\ * & * & P_p^{6(f)} \end{bmatrix} > 0$ and $R_{pg} = \begin{bmatrix} R_{pg}^1 & R_{pg}^2 & R_{pg}^3 \\ * & R_{pg}^4 & R_{pg}^5 \\ * & * & R_{pg}^6 \end{bmatrix} > 0$, and suitable dimensioned matrices $\mathcal{X}_{g\zeta(t_n)} = \begin{bmatrix} X_{g\zeta(t_n)}^1 & X_{g\zeta(t_n)}^2 & X_{g\zeta(t_n)}^3 \\ X_{g\zeta(t_n)}^4 & X_{g\zeta(t_n)}^5 & X_{g\zeta(t_n)}^3 \\ X_{g\zeta(t_n)}^6 & X_{g\zeta(t_n)}^7 & X_{g\zeta(t_n)}^3 \end{bmatrix}$, $Y_{g\zeta(t_n)}$, $\overline{L}_{g\zeta(t_n)}$, and $\overline{K}_{g\zeta(t_n)}$, such that conditions (15) and (16) hold, and

$$\begin{bmatrix} \Gamma_{pg\zeta(t_n)}^1 & \Gamma_{pg\zeta(t_n)}^2 \\ * & \mathbf{sym}\{-\epsilon Y_{g\zeta(t_n)}\} \end{bmatrix} < 0 \tag{31}$$

where

$$\begin{aligned}
\Gamma_{pg\zeta(t_n)}^1 &= \begin{bmatrix} \Upsilon_{pg\zeta(t_n)} & \widehat{\Omega}_{pg\zeta(t_n)} \\ * & \Sigma_{g\zeta(t_n)} \end{bmatrix}\\
\Gamma_{pg\zeta(t_n)}^2 &= \Big[\epsilon\overline{K}_{g\zeta(t_n)}\ 0\ -\epsilon\overline{K}_{g\zeta(t_n)}\ 0\ 0\ 0\ \sqrt{\varphi_{p1}}B_p^{\top}X_{g\zeta(t_n)}^{1\top}\\
&\quad \sqrt{\varphi_{p1}}B_p^{\top}X_{g\zeta(t_n)}^{4\top}\ \sqrt{\varphi_{p1}}B_p^{\top}X_{g\zeta(t_n)}^{7\top}\ \cdots\\
&\quad \sqrt{\varphi_{pS_s}}B_p^{\top}X_{g\zeta(t_n)}^{1\top}\ \sqrt{\varphi_{pS_s}}B_p^{\top}X_{g\zeta(t_n)}^{4\top}\\
&\quad \sqrt{\varphi_{pS_s}}B_p^{\top}X_{g\zeta(t_n)}^{7\top}\Big]^{\top}\\
\widehat{\Omega}_{pg\zeta(t_n)} &= \Big[\widehat{\Omega}_{pg\zeta(t_n)}^{1\top}\ \ \widehat{\Omega}_{pg\zeta(t_n)}^{2\top}\ \ \widehat{\Omega}_{pg\zeta(t_n)}^{3\top}\ \ 0\Big]^{\top}\\
\widehat{\Omega}_{pg\zeta(t_n)}^1 &= \Big[\sqrt{\varphi_{p1}}\widehat{\Omega}_{pg\zeta(t_n)}^{11\top}\ \sqrt{\varphi_{p1}}\widehat{\Omega}_{pg\zeta(t_n)}^{12\top}\ \sqrt{\varphi_{p1}}\widehat{\Omega}_{pg\zeta(t_n)}^{13\top}\ \cdots\\
&\quad \sqrt{\varphi_{pS_s}}\widehat{\Omega}_{pg\zeta(t_n)}^{11\top}\ \sqrt{\varphi_{pS_s}}\widehat{\Omega}_{pg\zeta(t_n)}^{12\top}\ \sqrt{\varphi_{pS_s}}\widehat{\Omega}_{pg\zeta(t_n)}^{13\top}\Big]\\
\widehat{\Omega}_{pg\zeta(t_n)}^2 &= \Big[\sqrt{\varphi_{p1}}\widehat{\Omega}_{pg\zeta(t_n)}^{21}\ \sqrt{\varphi_{p1}}\widehat{\Omega}_{pg\zeta(t_n)}^{22}\ \sqrt{\varphi_{p1}}\widehat{\Omega}_{pg\zeta(t_n)}^{23}\ \cdots\\
&\quad \sqrt{\varphi_{pS_s}}\widehat{\Omega}_{pg\zeta(t_n)}^{21}\ \sqrt{\varphi_{pS_s}}\widehat{\Omega}_{pg\zeta(t_n)}^{22}\ \sqrt{\varphi_{pS_s}}\widehat{\Omega}_{pg\zeta(t_n)}^{23}\Big]\\
\widehat{\Omega}_{pg\zeta(t_n)}^3 &= \Big[\sqrt{\varphi_{p1}}\widehat{\Omega}_{pg\zeta(t_n)}^{31}\ \sqrt{\varphi_{p1}}\widehat{\Omega}_{pg\zeta(t_n)}^{32}\ \sqrt{\varphi_{p1}}\widehat{\Omega}_{pg\zeta(t_n)}^{33}\ \cdots\\
&\quad \sqrt{\varphi_{pS_s}}\widehat{\Omega}_{pg\zeta(t_n)}^{31}\ \sqrt{\varphi_{pS_s}}\widehat{\Omega}_{pg\zeta(t_n)}^{32}\ \sqrt{\varphi_{pS_s}}\widehat{\Omega}_{pg\zeta(t_n)}^{33}\Big]\\
\widehat{\Omega}_{pg\zeta(t_n)}^{11} &= \Big[X_{g\zeta(t_n)}^1 A_p + X_{g\zeta(t_n)}^2\Phi_{\zeta(t_n)}C_p + \overline{L}_{g\zeta(t_n)}\big(I_{n_y}\\
&\quad - \Phi_{\zeta(t_n)}\big)C_p\ \ X_{g\zeta(t_n)}^2\big(I_{n_y} - \Phi_{\zeta(t_n)}\big) - \overline{L}_{g\zeta(t_n)}\\
&\quad \times\big(I_{n_y} - \Phi_{\zeta(t_n)}\big)\ \ X_{g\zeta(t_n)}^3 A_p - \overline{L}_{g\zeta(t_n)}C_p\Big]\\
\widehat{\Omega}_{pg\zeta(t_n)}^{12} &= \Big[X_{g\zeta(t_n)}^4 A_p + X_{g\zeta(t_n)}^5\Phi_{\zeta(t_n)}C_p + \overline{L}_{g\zeta(t_n)}\big(I_{n_y}\\
&\quad - \Phi_{\zeta(t_n)}\big)C_p\ \ X_{g\zeta(t_n)}^5\big(I_{n_y} - \Phi_{\zeta(t_n)}\big) - \overline{L}_{g\zeta(t_n)}\\
&\quad \times\big(I_{n_y} - \Phi_{\zeta(t_n)}\big)\ \ X_{g\zeta(t_n)}^3 A_p - \overline{L}_{g\zeta(t_n)}C_p\Big]\\
\widehat{\Omega}_{pg\zeta(t_n)}^{13} &= \Big[X_{g\zeta(t_n)}^6 A_p + X_{g\zeta(t_n)}^7\Phi_{\zeta(t_n)}C_p + \overline{L}_{g\zeta(t_n)}\big(I_{n_y}\\
&\quad - \Phi_{\zeta(t_n)}\big)C_p\ \ X_{g\zeta(t_n)}^7\big(I_{n_y} - \Phi_{\zeta(t_n)}\big) - \overline{L}_{g\zeta(t_n)}\\
&\quad \times\big(I_{n_y} - \Phi_{\zeta(t_n)}\big)\ \ X_{g\zeta(t_n)}^3 A_p - \overline{L}_{g\zeta(t_n)}C_p\Big]\\
\widehat{\Omega}_{pg\zeta(t_n)}^{21} &= -X_{g\zeta(t_n)}^2\Phi_{\zeta(t_n)} + \overline{L}_{g\zeta(t_n)}\Phi_{\zeta(t_n)}\\
\widehat{\Omega}_{pg\zeta(t_n)}^{22} &= -X_{g\zeta(t_n)}^5\Phi_{\zeta(t_n)} + \overline{L}_{g\zeta(t_n)}\Phi_{\zeta(t_n)}\\
\widehat{\Omega}_{pg\zeta(t_n)}^{23} &= -X_{g\zeta(t_n)}^7\Phi_{\zeta(t_n)} + \overline{L}_{g\zeta(t_n)}\Phi_{\zeta(t_n)}\\
\widehat{\Omega}_{pg\zeta(t_n)}^{31} &= X_{g\zeta(t_n)}^1 E_p + X_{g\zeta(t_n)}^3 E_p\\
\widehat{\Omega}_{pg\zeta(t_n)}^{32} &= X_{g\zeta(t_n)}^4 E_p + X_{g\zeta(t_n)}^3 E_p\\
\widehat{\Omega}_{pg\zeta(t_n)}^{33} &= X_{g\zeta(t_n)}^6 E_p + X_{g\zeta(t_n)}^3 E_p
\end{aligned}$$

and other matrices are provided in Theorem 1.

Meanwhile, the desired asynchronous gain matrices are given by

$$\begin{aligned}
L_{g\zeta(t_n)} &= \Big(X_{g\zeta(t_n)}^3\Big)^{-1}\overline{L}_{g\zeta(t_n)}\\
K_{g\zeta(t_n)} &= Y_{g\zeta(t_n)}^{-1}\overline{K}_{g\zeta(t_n)}.
\end{aligned} \tag{32}$$

Proof: By means of Lemma 1 and letting $\overline{L}_{g\zeta(t_n)} = X_{g\zeta(t_n)}^3 L_{g\zeta(t_n)}$ and $\overline{K}_{g\zeta(t_n)} = Y_{g\zeta(t_n)}K_{g\zeta(t_n)}$, Theorem 2 can be easily attained. This completes the proof. ■

IV. Illustrative Example

Example 1 (Numerical Example): Consider the MSS (1) with parameters

$$\begin{aligned}
A_1 &= \begin{bmatrix} 0.27 & -0.72 \\ 0.35 & 0.54 \end{bmatrix}, A_2 = \begin{bmatrix} 0.35 & -0.10 \\ 0.88 & -0.79 \end{bmatrix}\\
B_1 &= \begin{bmatrix} 0.19 \\ -0.57 \end{bmatrix}, B_2 = \begin{bmatrix} 2.06 \\ -0.66 \end{bmatrix}, E_1 = \begin{bmatrix} 0.1 \\ 0.1 \end{bmatrix}\\
E_2 &= \begin{bmatrix} 0.1 \\ 0.2 \end{bmatrix}, C_1 = C_2 = \begin{bmatrix} 1 & 1 \\ 1 & 1 \end{bmatrix}\\
F_1 &= [0.33\ \ -0.43], F_2 = [0.57\ 0.18].
\end{aligned}$$

The transition probability matrix is given by $\Pi = \begin{bmatrix} 0.5 & 0.5 \\ 0.05 & 0.95 \end{bmatrix}$, and let $\beta_\iota = \{1, 2\}$ ($\iota \geq 0$), the detection probabilities of the actual mode are assumed to be

$$\Psi^{(1)} = \begin{bmatrix} 0.52 & 0.48 \\ 0.25 & 0.75 \end{bmatrix}, \Psi^{(1)} = \begin{bmatrix} 0.52 & 0.48 \\ 0.25 & 0.75 \end{bmatrix}.$$

Aiming to construct the observer-based controller and selecting $\eta = 50$, $\upsilon = 0.6$, $\theta = 0.5$ and $\epsilon = 0.6$, $\kappa_{\zeta(t_n),1} = 0.6$, $\kappa_{\zeta(t_n),2} = 0.4$, and $\overline{Q} = \text{diag}\{0.05, 0.1\}$.

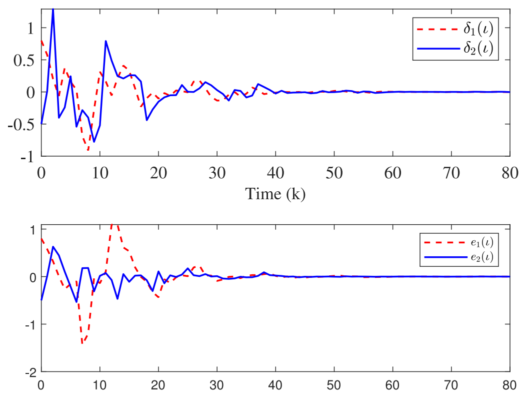

Fig. 2. State trajectories $\delta(\iota)$ and $e(\iota)$ in Example 1.

TABLE I
PARAMETER MEANING

Parameter	Physical Meaning
l	the robot arm length
g	the gravity acceleration
$\mathscr{M}$	the payload mass
$\mathscr{J}$	the inertia moment
$\mathscr{R}$	the viscous friction coefficient

Choosing $\gamma = 1.8$, by solving the LMIs in Theorem 2, the desired controller gain matrices can be achieved

$$\begin{bmatrix} L_{11} \\ \hline L_{21} \end{bmatrix} = \left[\begin{array}{cc} -0.0063 & -0.3299 \\ -0.2231 & 0.4508 \\ \hline -0.1453 & -0.0129 \\ -0.6961 & 0.6192 \end{array}\right]$$

$$\begin{bmatrix} L_{12} \\ \hline L_{22} \end{bmatrix} = \left[\begin{array}{cc} 0.2329 & -0.5453 \\ -0.0752 & 0.2792 \\ \hline 0.4070 & -0.5432 \\ -0.0600 & -0.0286 \end{array}\right]$$

$$\begin{bmatrix} K_{11} \\ \hline K_{21} \end{bmatrix} = \left[\begin{array}{cc} 0.0039 & -0.0006 \\ \hline 0.0033 & -0.0004 \end{array}\right]$$

$$\begin{bmatrix} K_{12} \\ \hline K_{22} \end{bmatrix} = \left[\begin{array}{cc} -0.0053 & 0.0092 \\ \hline -0.0076 & 0.0068 \end{array}\right].$$

To verify the effectiveness of the designed observer-based controller, selecting the initial states $\delta(0) = [0.9 \quad -0.45]^\top$ and $\widehat{\delta}(0) = [0 \ 0]^\top$. The simulation results can be presented in Figs. 2–6. The evolutions of state trajectories of $\delta(\iota)$ and $e(\iota)$ are shown in Fig. 2, and the control input is depicted in Fig. 3. Furthermore, the evolutions of the state trajectories of $y(\iota)$ and $\bar{y}(\iota)$ are plotted in Fig. 4. Besides, the internal dynamic state $\Im(\iota)$ is illustrated in Fig. 5, and the dynamic event-based release interval is depicted in Fig. 6. Define

$$\text{Triggering rate} = \frac{\text{The number of the transmitted packages}}{\text{The total number of sampled data packages}}$$

In this case, the triggering rate is $50/80 \approx 62.50\%$.

Example 2 (Practical Example): A single-link robot arm model (SLRAM) [33] is applied to verify the applicability and effectiveness of the proposed methodology. The dynamic

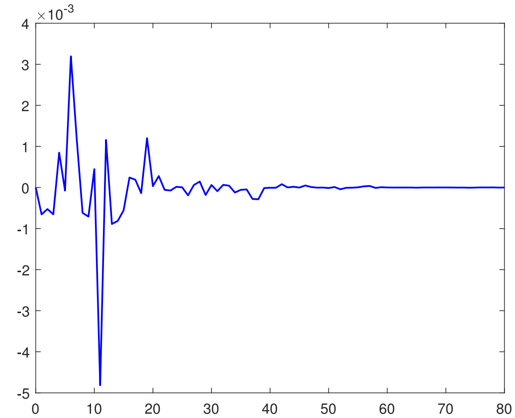

Fig. 3. Control input in Example 1.

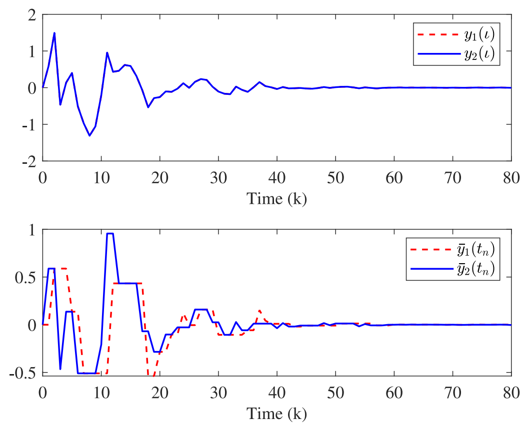

Fig. 4. State trajectories $y(\iota)$ and $\bar{y}(\iota)$ in Example 1.

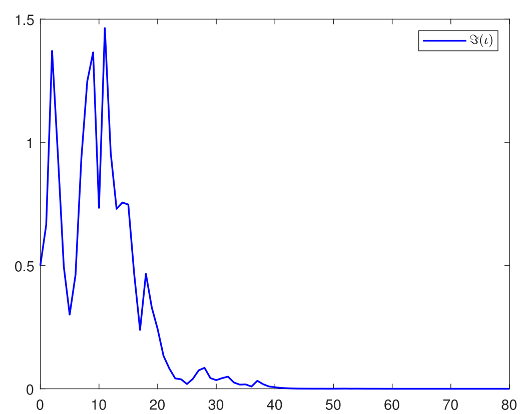

Fig. 5. Internal dynamic state $\Im(\iota)$ in Example 1.

TABLE II
VALUES $\mathscr{M}(\alpha_\iota)$ AND $\mathscr{J}(\alpha_\iota)$ FOR DIFFERENT α_ι

α_ι	1	2	3
$\mathscr{M}(\alpha_\iota)$	1	5	10
$\mathscr{J}(\alpha_\iota)$	1	5	10

equations of SLRAM can be modeled as follows:

$$\begin{cases} \dot{\delta}_1(t) = \delta_2(t) \\ \dot{\delta}_2(t) = -\frac{gl\mathscr{M}}{\mathscr{J}}\sin(\delta_1(t)) - \frac{\mathscr{R}}{\mathscr{J}}\delta_2(t) + \frac{1}{\mathscr{J}}u(t) \end{cases} \tag{33}$$

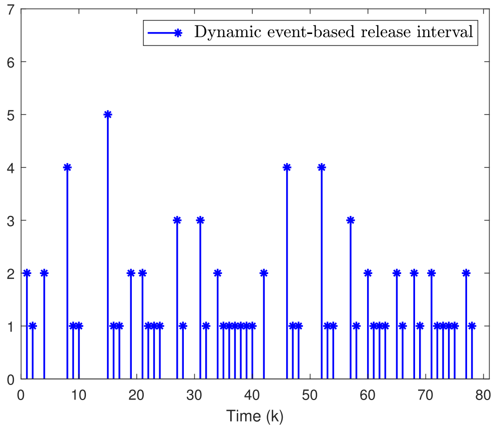

Fig. 6. DETS with Example 1.

where $\delta_1(t) = \theta(t)$ and $\delta_2(t) = \dot{\theta}(t)$ signify the angle and angular velocity of the SLRAM, respectively. The physical meaning of l, g, $\mathscr{R}$, $\mathscr{M}$, and $\mathscr{J}$ are given in Table I. One assumes that $\mathscr{L} = 0.5$, $g = 9.81$, and $\mathscr{R} = 2$. In this example, assuming the SLRAM has three different modes, and the values of parameters $\mathscr{M}_k$ and $\mathscr{J}_k$ are given in Table II. By the sampling period $T = 0.1$, (33) can be rewritten as

$$\begin{cases} \delta(\iota+1) = A_p\delta(\iota) + B_p u(\iota) + E_p\omega(\iota) \\ y(\iota) = C_p\delta(\iota) \\ z(\iota) = F_p\delta(\iota) \end{cases}$$

where

$$A(\alpha_\iota) = \begin{bmatrix} 1 & T \\ -\frac{Tgl\mathscr{M}(\alpha_\iota)}{\mathscr{J}(\alpha_\iota)} & 1 - \frac{T\mathscr{R}(\alpha_\iota)}{\mathscr{J}(\alpha_\iota)} \end{bmatrix}$$

$$B(\alpha_\iota) = \begin{bmatrix} 0 \\ \frac{T}{\mathscr{J}(\alpha_\iota)} \end{bmatrix}, E(\alpha_\iota) = [0 \quad T]^\top, \quad (\alpha_\iota = 1, 2, 3).$$

Other parameters are given as $\{C(\alpha_\iota)\}_{\iota=1}^3 = \begin{bmatrix} 0.2 & 0 \\ -1 & 0 \end{bmatrix}$, $F(\alpha_\iota) = [1 \quad 1]$, $\kappa_{\zeta(t_n),1} = 0.7$, $\kappa_{\zeta(t_n),2} = 0.3$, $\overline{Q} = \mathrm{diag}\{0.15, 0.15\}$, $\upsilon = 0.8$, $\theta = 0.5$, and $\eta = 40$.

The transition probability matrix of the actual mode is elicited as

$$\Pi = \begin{bmatrix} 0.4 & 0.3 & 0.3 \\ 0.1 & 0.5 & 0.4 \\ 0.6 & 0.2 & 0.2 \end{bmatrix}.$$

On the other hand, the asynchronous observer-based controller is also involved in three modes, which means the hidden switching mode $\beta_\iota = \{1, 2, 3\}(\iota \geq 0)$. The detection probabilities are nonhomogeneous, and its detection probability matrices $\Psi^{(l)}$ are selected as

$$\Psi^{(1)} = \begin{bmatrix} 0.32 & 0.4 & 0.28 \\ 0.05 & 0.45 & 0.5 \\ 0.66 & 0.22 & 0.12 \end{bmatrix}, \quad \Psi^{(2)} = \begin{bmatrix} 0.52 & 0.08 & 0.4 \\ 0.25 & 0.45 & 0.3 \\ 0.6 & 0.1 & 0.3 \end{bmatrix}.$$

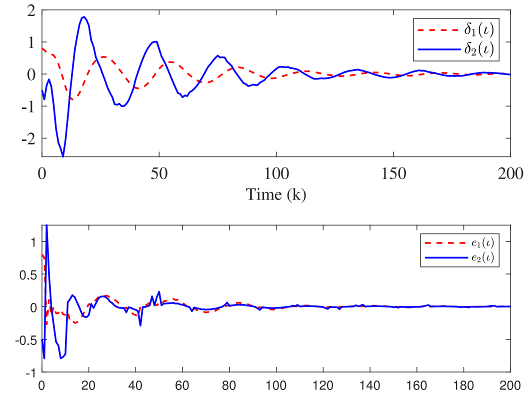

Fig. 7. State trajectories $\delta(\iota)$ and $e(\iota)$ with $\eta = 40$ in Example 2.

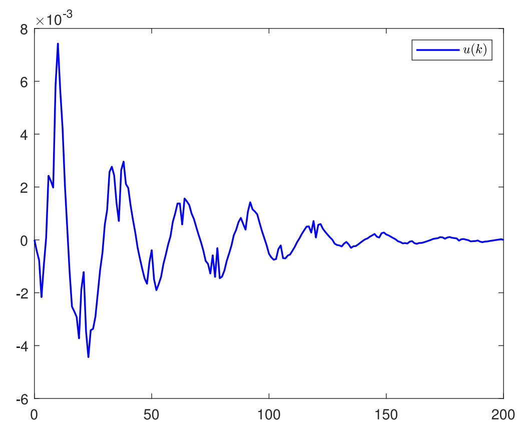

Fig. 8. Control input with $\eta = 40$ in Example 2.

Selecting $\gamma = 6.5$, by solving the LMIs in Theorem 2, the desired controller gain matrices can be obtained

$$\begin{bmatrix} L_{11} \\ \hline L_{21} \\ \hline L_{31} \end{bmatrix} = \left[\begin{array}{cc} 1.0142 & -0.3929 \\ 1.5887 & 0.0153 \\ \hline 0.9974 & -0.3497 \\ 1.4658 & 0.0192 \\ \hline 1.0019 & -0.3650 \\ 1.5022 & 0.0194 \end{array}\right]$$

$$\begin{bmatrix} L_{12} \\ \hline L_{22} \\ \hline L_{32} \end{bmatrix} = \left[\begin{array}{cc} 1.1408 & -0.3706 \\ 3.9468 & 0.6055 \\ \hline 1.0669 & -0.3344 \\ 3.6829 & 0.6357 \\ \hline 1.0749 & -0.3441 \\ 3.6818 & 0.6297 \end{array}\right]$$

$$\begin{bmatrix} K_{11} \\ \hline K_{21} \\ \hline K_{31} \end{bmatrix} = \left[\begin{array}{cc} -0.0038 & -0.0019 \\ \hline -0.0038 & -0.0021 \\ \hline -0.0041 & -0.0022 \end{array}\right]$$

$$\begin{bmatrix} K_{12} \\ \hline K_{22} \\ \hline K_{32} \end{bmatrix} = \left[\begin{array}{cc} 0.0019 & -0.0009 \\ \hline 0.0019 & -0.0009 \\ \hline 0.0021 & -0.0009 \end{array}\right].$$

Selecting the initial states $\delta(0) = [0.8 \quad -0.5]^\top$ and $\widehat{\delta}(0) = [0\ 0]^\top$, we choose $\omega(\iota) = 10\exp(-0.1\iota)\cos(0.5\iota)$. For $\eta = 40$, the simulation results can be observed in Figs. 7–11. The evolutions of state trajectories of $\delta(\iota)$ and $e(\iota)$ are shown in Fig. 7, and control input $u(k)$ is depicted in Fig. 8. Meanwhile,

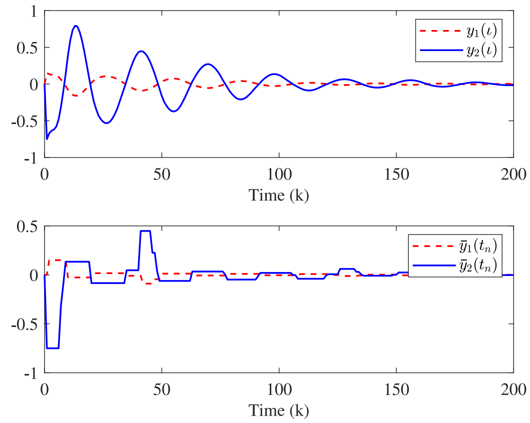

Fig. 9. State trajectories $y(\iota)$ and $\bar{y}(\iota)$ with $\eta = 40$ in Example 2.

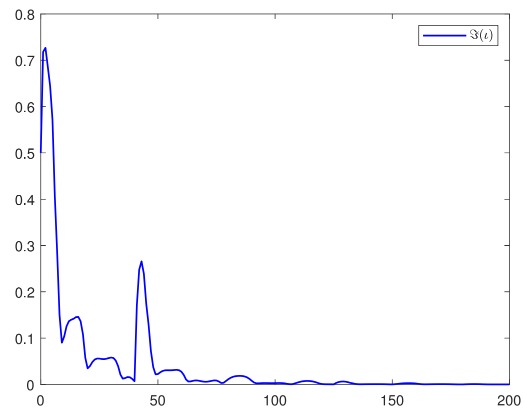

Fig. 10. Internal dynamic state $\Im(\iota)$ with $\eta = 40$ in Example 2.

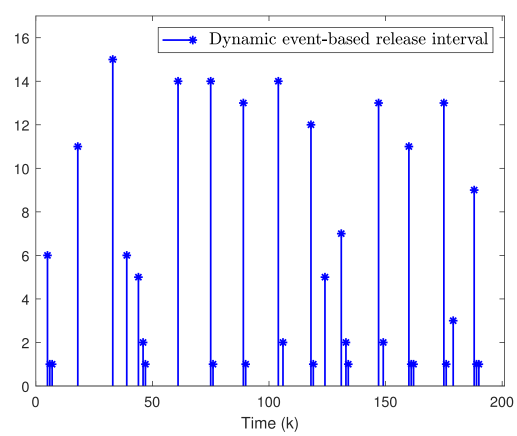

Fig. 11. DETS with $\eta = 40$ in Example 2.

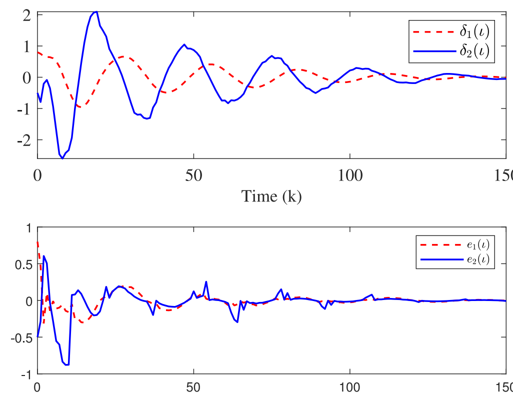

Fig. 12. State trajectories $\delta(\iota)$ and $e_(\iota)$ with $\eta = 100$ in Example 2.

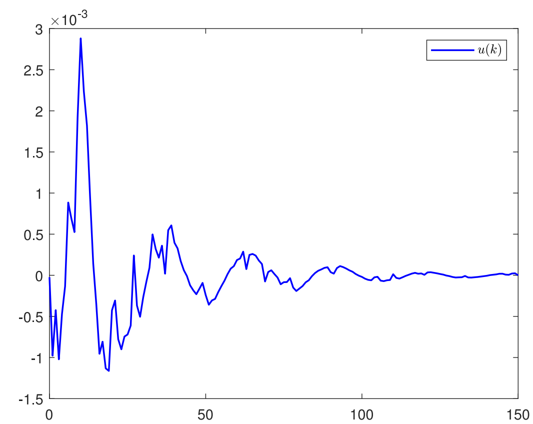

Fig. 13. Control input with $\eta = 100$ in Example 2.

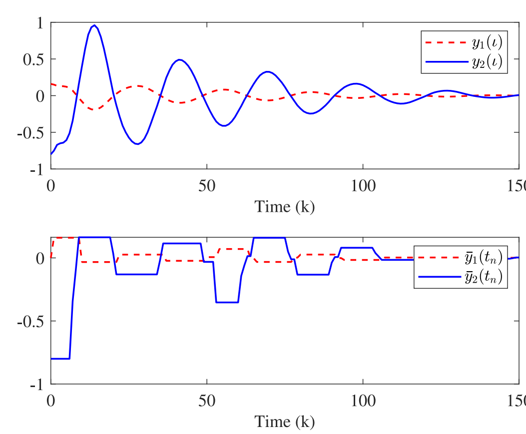

Fig. 14. State trajectories $y(\iota)$ and $\bar{y}(\iota)$ with $\eta = 100$ in Example 2.

the evolutions of the state trajectories of $y(\iota)$ and $\bar{y}(\iota)$ are plotted in Fig. 9. Besides, the internal dynamic state $\Im(\iota)$ is illustrated in Fig. 10, and the dynamic event-based release interval is depicted in Fig. 11. In this case, the triggering time is 34, which means the triggering rate is $34/200 \approx 17\%$. On the other hand, for $\eta = 100$, the simulation results can be observed in Figs. 12–16. The evolutions of state trajectories of $\delta(\iota)$ and $e(\iota)$ are shown in Fig. 12, and control input is presented in Fig. 13. The evolutions of the state trajectories of $y(\iota)$ and $\bar{y}(\iota)$ are plotted in Fig. 14. Besides, the internal dynamic state $\Im(\iota)$ is illustrated in Fig. 15, and the dynamic event-based release interval is depicted in Fig. 16. In this case, the triggering time is 29, which means the triggering rate is $29/150 \approx 19.33\%$. Apparently, the bigger η may result in a higher triggering rate. Disclosed from the aforementioned figures, one can conclude that the attained methodology is effective.

V. Conclusion

In this study, the asynchronous filtering of discrete-time MSS has been studied. To avoid the data collisions and

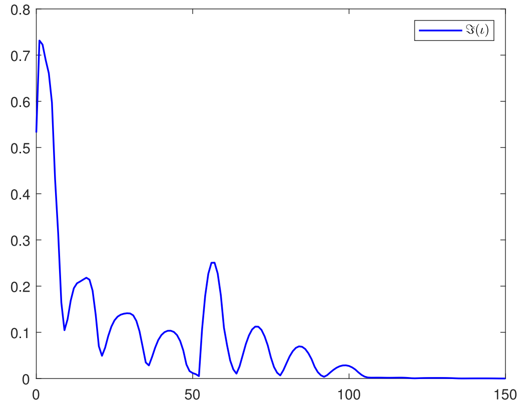

Fig. 15. Internal dynamic state $\Im(\iota)$ with $\eta = 100$ in Example 2.

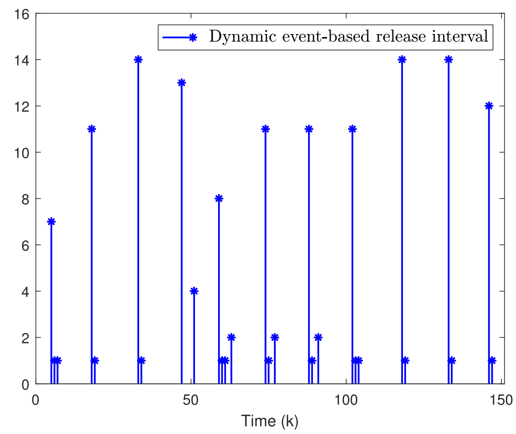

Fig. 16. DETS with $\eta = 100$ in Example 2.

side effects in a constrained communication channel, a novel DEWTOD protocol was proposed for the controller design. By resorting to the hidden Markov model and polytopic-structured Lyapunov-functional, sufficient conditions are derived such that the closed-loop dynamic is MSES. Finally, two examples were provided to explicate the validity of the derived results. Furthermore, for practical systems with time-varying delays, the computational complexity may be increased, how to extend the derived results to time-delayed MSSs will be exploited in future works. Meanwhile, future work will also include the complex control issue with asynchronous phenomena, such as trajectory tracking control [34], adaptive event trigger [35], and iterative learning control [36].

REFERENCES

[1] L. Zhang, Y. Zhu, and W. X. Zheng, "State estimation of discrete-time switched neural networks with multiple communication channels," *IEEE Trans. Cybern.*, vol. 47, no. 4, pp. 1028–1040, Apr. 2017.

[2] L. Liu, Y. J. Liu, A. Chen, S. Tong, and C. L. P. Chen, "Integral barrier Lyapunov function based adaptive control for switched nonlinear systems," *Sci. China Inf. Sci.*, vol. 63, no. 3, 2020, Art. no. 132203.

[3] J. H. Park, H. Shen, X. H. Chang, T. H. Lee, *Recent Advances in Control and Filtering of Dynamic Systems With Constrained Signals*. Cham, Switzerland: Springer, 2018, doi: 10.1007/978-3-319-96202-3.

[4] S. Pan, Z. Ye, and J. Zhou, "Fault detection filtering for a class of nonhomogeneous Markov jump systems with random sensor saturations," *Int. J. Control Autom. Syst.*, vol. 18, no. 2, pp. 439–449, 2020.

[5] J. Cheng, W. Huang, H. K. Lam, J. Cao, and Y. Zhang, "Fuzzy-model-based control for singularly perturbed systems with nonhomogeneous Markov switching: A dropout compensation strategy," *IEEE Trans. Fuzzy Syst.*, early access, Dec. 1, 2020, doi: 10.1109/TFUZZ.2020.3041588.

[6] Y. Zhu, X. Song, M. Wang, and J. Lu, "Finite-time asynchronous $\mathcal{H}_\infty$ filtering design of Markovian jump systems with randomly occurred quantization," *Int. J. Control Autom. Syst.*, vol. 18, no. 2, pp. 450–461, 2020.

[7] S. Aberkane, "Stochastic stabilization of a class of nonhomogeneous Markovian jump linear systems," *Syst. Control Lett.*, vol. 60, no. 3, pp. 156–160, 2011.

[8] S. Tong, X. Min, and Y. Li, "Observer-based adaptive fuzzy tracking control for strict-feedback nonlinear systems with unknown control gain functions," *IEEE Trans. Cybern.*, vol. 50, no. 9, pp. 3903–3913, Sep. 2020.

[9] Y. Li, X. Min, and S. Tong, "Observer-based fuzzy adaptive inverse optimal output feedback control for uncertain nonlinear systems," *IEEE Trans. Fuzzy Syst.*, vol. 29, no. 6, pp. 1484–1495, Jun. 2021, doi: 10.1109/TFUZZ.2020.2979389.

[10] L. Liu, T. Gao, Y. J. Liu, S. Tong, C. L. P. Chen, and L. Ma, "Time-varying IBLF based on adaptive control of uncertain nonlinear systems with full state constraints," *Automatica*, to be published, doi: 10.1016/j.automatica.2021.

[11] Y. Wang, H. Pu, P. Shi, C. K. Ahn, and J. Luo, "Sliding mode control for singularly perturbed Markov jump descriptor Systems with nonlinear perturbation," *Automatica*, vol. 127, May 2021, Art. no. 109515.

[12] J. Cheng, Y. Shan, J. Cao, and J. H. Park, "Nonstationary control for T-S fuzzy Markovian switching systems with variable quantization density," *IEEE Trans. Fuzzy Syst.*, vol. 29, no. 6, pp. 1375–1385, Jun. 2021.

[13] J. Cheng, J. H. Park, X. Zhao, H. R. Karimi, and J. Cao, "Quantized nonstationary filtering of network-based Markov switching RSNSs: A multiple hierarchical structure strategy," *IEEE Trans. Autom. Control*, vol. 65, no. 11, pp. 4816–4823, Nov. 2020.

[14] Y. Shen, Z. G. Wu, P. Shi, and C. K. Ahn, "Model reduction of Markovian jump systems with uncertain probabilities," *IEEE Trans. Autom. Control*, vol. 65, no. 1, pp. 382–388, Jan. 2020.

[15] M. Liu and G. Wang, "Observer-based controller design for discrete-time Markovian jump linear systems with partial information," *IEEE Access*, vol. 7, pp. 41145–41153, 2019.

[16] Z.G. Wu, S. Dong, H. Su, and C. Li, "Asynchronous dissipative control for fuzzy Markov jump systems," *IEEE Trans. Cybern.*, vol. 48, no. 8, pp. 2426–2436, Aug. 2018.

[17] Y. Xu, Z.-G. Wu, Y.-J. Pan, and J. Sun, "Resilient asynchronous state estimation for Markovian jump neural networks subject to stochastic nonlinearities and sensor saturations," *IEEE Trans. Cybern.*, early access, Jan. 8, 2021, doi: 10.1109/TCYB.2020.3042473.

[18] M. Abdelrahim, V. Dolk, and W. P. M. H. Heemels, "Event-triggered quantized control for input-to-state stabilization of linear systems with distributed output sensors," *IEEE Trans. Autom. Control*, vol. 64, pp. 4952–4967, Dec. 2019.

[19] Y. Yuan, Z. Wang, and L. Guo, "Event-triggered strategy design for discrete-time nonlinear quadratic games with disturbance compensations: The noncooperative case," *IEEE Trans. Syst., Man, Cybern., Syst.*, vol. 48, no. 11, pp. 1885–1896, Nov. 2018.

[20] L. Wu, Y. Gao, J. Liu, and H. Li, "Event-triggered sliding mode control of stochastic systems via output feedback," *Automatica*, vol. 82, pp. 79–92, Aug. 2017.

[21] H. Yan, H. Zhang, F. Yang, X. Zhan, and C. Peng, "Event-triggered asynchronous guaranteed cost control for Markov jump discretetime neural networks with distributed delay and channel fading," *IEEE Trans. Neural Netw. Learn. Syst.*, vol. 29, no. 8, pp. 3588–3598, Aug. 2018.

[22] J. Xu, D. W. C. Ho, F. Li, W. Yang, and Y. Tang, "Event-triggered risk-sensitive state estimation for hidden Markov models," *IEEE Trans. Autom. Control*, vol. 64, no. 10, pp. 4276–4283, Oct. 2019.

[23] H. Yan, J. Sun, H. Zhang, X. Zhan, and F. Yang, "Event-triggered $\mathcal{H}_\infty$ state estimation of 2-DOF quarter-car suspension systems with nonhomogeneous Markov switching," *IEEE Trans. Syst., Man, Cybern., Syst.*, vol. 50, no. 9, pp. 3320–3329, Sep. 2020.

[24] A. Girard, "Dynamic triggering mechanisms for event-triggered control," *IEEE Trans. Autom. Control*, vol. 60, no. 7, pp. 1992–1997, Jul. 2015.

[25] J. Song and Y. Niu, "Dynamic dvent-triggered sliding mode control: Dealing with slow sampling singularly perturbed systems," *IEEE Trans. Circuits Syst. II, Exp. Briefs*, vol. 67, no. 6, pp. 1079–1083, Jun. 2020.

[26] H. Dong, Z. Wang, B. Shen, and D. Ding, "Variance-constrained $\mathcal{H}_\infty$ control for a class of nonlinear stochastic discrete time-varying systems: The event-triggered design," *Automatica*, vol. 72, pp. 28–36, Oct. 2016.

[27] H. Shen, Y. Men, J. Cao, and J. H. Park, "$\mathcal{H}_\infty$ filtering for fuzzy jumping genetic regulatory networks with round-robin protocol: A hidden-Markov-model-based approach," *IEEE Trans. Fuzzy Syst.*, vol. 28, no. 1, pp. 112–121, Jan. 2020.

[28] L. Zou, Z. Wang, H. Gao, and F. E. Alsaadi, "Finite-horizon $\mathcal{H}_\infty$ consensus control of time-varying multiagent systems with stochastic communication protocol," *IEEE Trans. Cybern.*, vol. 47, no. 8, pp. 1830–1840, Aug. 2017.

[29] L. Zou, Z. Wang, Q. L. Han, and D. Zhou, "Ultimate boundedness control for networked systems with try-once-discard protocol and uniform quantization effects," *IEEE Trans. Autom. Control*, vol. 62, no. 12, pp. 6582–6588, Dec. 2017.

[30] Y. Dong, Y. Song, J. Wang, and B. Zhang, "Dynamic output-feedback fuzzy MPC for Takagi-Sugeno fuzzy systems under event-triggering-based try-once-discard protocol," *Int. J. Robust Nonlinear Control*, vol. 30, no. 4, pp. 1394–1416, 2020.

[31] J. Han, H. Zhang, Y. Wang, and K. Zhang, "Fault estimation and fault-tolerant control for switched fuzzy stochastic systems," *IEEE Trans. Fuzzy Syst.*, vol. 26, no. 5, pp. 2993–3003, Oct. 2018.

[32] S. Dong, M. Fang, and S. Chen, "Extended dissipativity asynchronous static output feedback control of Markov jump systems," *Inf. Sci.*, vol. 514, pp. 275–287, Apr. 2020.

[33] H.-N. Wu and K.-Y. Cai, "Mode-independent robust stabilization for uncertain Markovian jump nonlinear systems via fuzzy control," *IEEE Trans. Syst., Man, Cybern. B, Cybern.*, vol. 36, no. 3, pp. 509–519, Jun. 2006.

[34] W. He, X. Mu, L. Zhang, and Y. Zou, "Modeling and trajectory tracking control for flapping-wing micro aerial vehicles," *IEEE/CAA J. Automatica Sinica*, vol. 8, no. 1, pp. 148–156, Jan. 2021.

[35] L. Liu, X. Li, Y.-J. Liu, and S. Tong, "Neural network based adaptive event trigger control for a class of electromagnetic suspension systems," *Control Eng. Pract.*, vol. 106, Jan. 2021, Art. no. 104675.

[36] W. He, T. Meng, X. He, and C. Sun, "Iterative learning control for a flapping wing micro aerial vehicle under distributed disturbances," *IEEE Trans. Cybern.*, vol. 49, no. 4, pp. 1524–1535, Apr. 2019.

Jun Cheng received the B.S. degree from the Hubei University for Nationalities, Enshi City, Hubei, China, in 2010, and the Ph.D. degree from the University of Electronic Science and Technology of China, Chengdu, China, in 2015.

From 2015 to 2019, he is a Staff Member with the Hubei University for Nationalities. He was a Visiting Scholar with the Department of Electrical and Computer Engineering, National University of Singapore, Singapore, from 2013 to 2014, and the Department of Electrical Engineering, Yeungnam University, Gyeongsan, South Korea, in 2016 and 2018. Since 2019, he has been with the Guangxi Normal University, Guilin, China, where he is currently a Professor with the School of Mathematics and Statistics, Center for Applied Mathematics of Guangxi. His current research interests include analysis and synthesis for stochastic hybrid systems, networked control systems, robust control, and nonlinear systems.

Dr. Cheng has been a recipient of Highly Cited Researcher Award listed by Clarivate Analytics in 2019 and 2020. He serves as an Associate Editor of the *International Journal of Control, Automation, and Systems*.

Ju H. Park (Senior Member, IEEE) received the Ph.D. degree in electronics and electrical engineering from Pohang University of Science and Technology (POSTECH), Pohang, South Korea, in 1997.

From May 1997 to February 2000, he was a Research Associate with the Engineering Research Center-Automation Research Center, POSTECH. He joined Yeungnam University, Gyeongsan, South Korea, in March 2000, where he is currently the Chuma Chair Professor. He has coauthored the monographs *Recent Advances in Control and Filtering of Dynamic Systems With Constrained Signals* (New York, NY, USA: Springer–Nature, 2018) and *Dynamic Systems With Time Delays: Stability and Control* (New York, NY, USA: Springer–Nature, 2019) and is an Editor of an edited volume *Recent Advances in Control Problems of Dynamical Systems and Networks* (New York: Springer–Nature, 2020). His research interests include robust control and filtering, neural/complex networks, fuzzy systems, multiagent systems, and chaotic systems. He has published a number of articles in the above areas.

Prof. Park has been a recipient of the Highly Cited Researchers Award by Clarivate Analytics (formerly, Thomson Reuters), since 2015, and listed in three fields, Engineering, Computer Sciences, and Mathematics, in 2019 and 2020. He also serves as an Editor for the *International Journal of Control, Automation and Systems*. He is also a Subject Editor/Advisory Editor/Associate Editor/Editorial Board Member of several international journals, including *IET Control Theory & Applications*, *Applied Mathematics and Computation*, *Journal of The Franklin Institute*, *Nonlinear Dynamics*, *Engineering Reports*, *Cogent Engineering*, the IEEE TRANSACTION ON FUZZY SYSTEMS, the IEEE TRANSACTION ON NEURAL NETWORKS AND LEARNING SYSTEMS, and the IEEE TRANSACTION ON CYBERNETICS. He is a Fellow of the Korean Academy of Science and Technology.

Zheng-Guang Wu (Member, IEEE) was born in 1982. He received the B.S. and M.S. degrees in mathematics from Zhejiang Normal University, Jinhua, China, in 2004 and 2007, respectively, and the Ph.D. degree in control science and engineering from Zhejiang University, Hangzhou, China, in 2011.

He has authored or coauthored over 100 papers in refereed international journals. His current research interests include hybrid systems, Markov jump systems, sampled-data systems, fuzzy systems, multiagent systems, Boolean control networks, stochastic systems, and neural networks.

Dr. Wu was named a Highly Cited Researcher (Clarivate Analytics). He serves as an Associate Editor/Editorial Board Member for some international journals, such as the IEEE TRANSACTIONS ON SYSTEMS, MAN AND CYBERNETICS: SYSTEMS; the *Journal of the Franklin Institute*; *Neurocomputing*; the *International Journal of Control, Automation, and Systems*; IEEE ACCESS; the *International Journal of Sensors, Wireless Communications and Control*; and IEEE Control Systems Society Conference Editorial Board. He is an Invited Reviewer of Mathematical Review of the American Mathematical Society.